

RICAL SIMULATION OF STRUCTURALLY INTEGRATED THERMAL PROTECTION APPLIED IN THE SARA SUB-ORBITAL PLATFORM

Humberto Araujo Machado

Manolo Pires

Institute of Aeronautics and Space - IAE, Praça Marechal Eduardo Gomes, 50, Vila das Acácias, São José dos Campos, SP, 12228-904

humbertoam@iae.cta.br

Ricardo Fortes de Miranda

Guilherme Barros Ameloti

Federal University of Uberlândia, School of Mechanical Engineering, Av. João Naves de Ávila, 2160, Campus Santa Mônica, Bloco 1M, Uberlândia, MG, 38400-902

Abstract. In this work, the use of a Thermally Integrated Structural Sandwich Core (TISSC), a new kind of space vehicle thermal protection, in the SARA sub-orbital platform, which is being developed by IAE/CTA for micro-gravity research, is proposed, replacing the conventional cork layer used as a TPS (Thermal Protection System). The advantages of using such a structure are its lightweight and the same insulation as load bearing capabilities, low maintenance, and low life-cycle cost. The aerodynamic heating of the vehicle is estimated during the ascendant period of the trajectory through numerical simulation, in order to obtain the resulting temperatures and heat fluxes. The thermal performances of the two systems are compared and results for maximum internal temperature are presented, were the equivalent thermal conductivity for the TISSC stuff is estimated through a well-established model.

Keywords: Thermal protection system, Aerodynamic heating, Structurally integrated thermal protection, Numerical simulation)

1. INTRODUCTION

Space and sub-orbital vehicles reach high velocities within atmosphere, about 100 km over Earth's surface. Such high velocities result in aerodynamic heating and air temperature surpasses 2000° C at the stagnation point. Besides the effects of high temperatures on the mechanical behavior of the structure and on-board devices, it is mandatory to preserve the payload, by using an efficient TPS (Thermal Protection System). As a consequence, TPS design is a critical aspect of a rocket design, since his under dimensioning may result in the loss of the payload and the over dimensioning implies in increasing weight and cost.

Sub-orbital platforms are a low-cost alternative for micro-gravity research. The SARA sub-orbital platform, Fig. 1, is being developed by IAE/DCTA for this application. Its mass is 250 kg for a payload of about 25 kg. The sub-orbital version is designed to provide 6 minutes of micro-gravity environment. In the future, the orbital version is expected to reach an orbit of 300 km around the Earth during 10 days (Moraes, 1998). It reaches the speed of 9300 km/h while still flying within the earth's atmosphere.

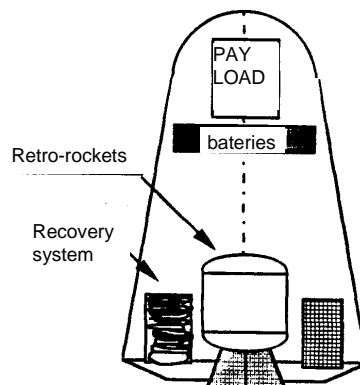


Figure 1. SARA sub-orbital platform and its internal systems.

A structural sandwich panel is a three-layer plate, consisting of two face sheets and a core. Two thin, stiff and strong faces are separated by a thick, light and weaker core. Such construction provides high strength-to-weight ratio and it promises high stiffness. Traditionally, sandwich structures are made up of two face sheets and a core that is made from expanded materials such as, metallic foil, plastic and composite in the shape of hexagons with vertical walls

H. A. Machado, M. Pires, R. F. Miranda, G. B. Ameloti
Structurally Integrated Thermal Protection Applied in the SARA

(honeycomb). As an option, Thermally Integrated Structural Sandwich Core (TISSC) would insulate the vehicle from aerodynamic heating as well as carry primary vehicle loads. The advantages of using such a structure are that it is lightweight, multifunctional, for example offer insulation as well as load bearing capabilities, low maintenance, and low life-cycle cost. The truss-core sandwich panel is comprised of several unit cells. The unit cell consists of two thin face sheets and an inclined web made up of composite laminates. Commonly used materials for facings and core are ceramic matrix composite laminates and metals. The composite truss core can be filled with Saffil, which is a non-load-bearing insulation made of aluminum fibers (Martinez et al, 2006).



Figure 2. Thermally Integrated Structural Sandwich Core (TISSC) – NASA concept.

In this work, the use of a TISSC in the SARA is proposed, replacing the conventional cork layer used as a TPS. The thermal performances of the two systems are compared and results for maximum temperatures are presented, were the equivalent thermal conductivity for the TISSC stuff is estimated through the model developed by Daryabeigi (2003).

2. PHYSICAL PROBLEM AND MATHEMATICAL MODEL

Figure 3 shows the lateral thermal protection of SARA. A 4 mm Aluminium wall is covered with a 6 mm cork layer. This protection is employed in the whole SARA conic section. The previous arrangement is replaced by a sandwich structure similar to Fig.2, with two Aluminium walls with 1 mm thickness, filled with a 18 mm Saffil layer, Fig. 4. The change in the total thickness is compatible with the slope of the semi-spherical top after a small adjustment.

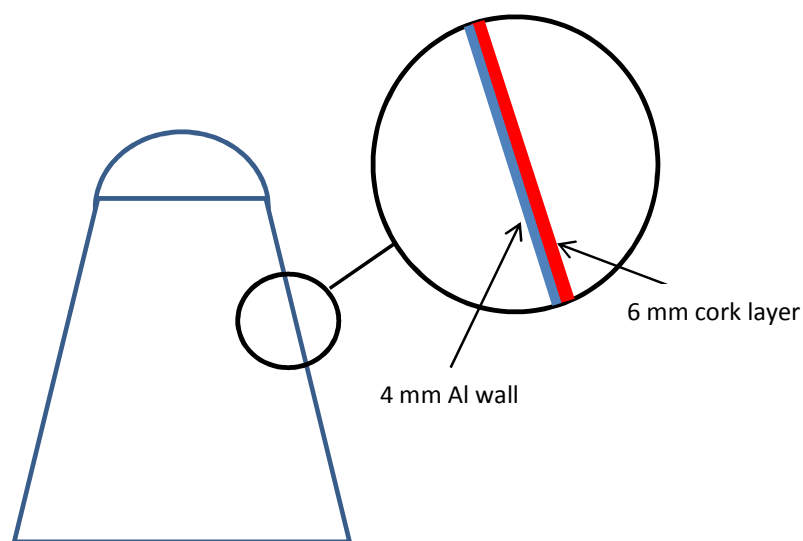


Figure 3. Lateral thermal protection of SARA wall.

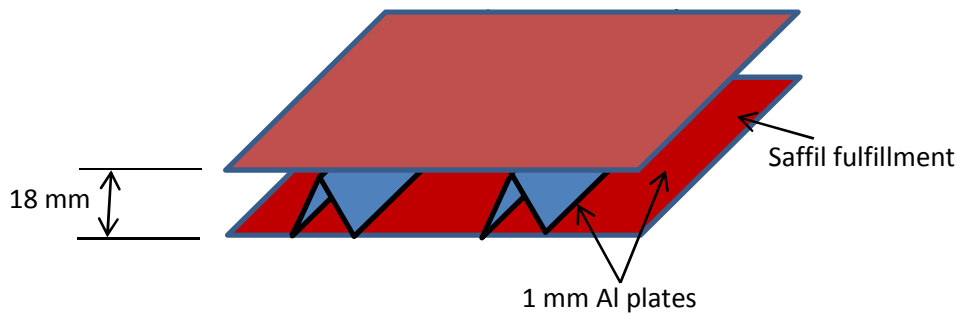


Figure 4. Schematics of the proposed arrangement for the integrated thermal protection

2.1 Aerodynamic heating

To predict the heat transfer on SARA, it is necessary to know pressure, temperature and velocity fields around the vehicle. That can be accomplished by numerically solving the N-S equations. However, such a procedure is expensive and time consuming. In the present work a simpler, but reliable, engineering approach is also used. The following simplifying assumptions are made:

- Zero angle of attack;
- SARA rotation around its longitudinal axis is neglected;
- Atmospheric air is considered to behave as a calorically and thermally perfect gas (no chemical reactions); and

The free stream conditions ahead of the nose cap are those given by v_∞ , T_∞ , p_∞ , corresponding, respectively, to velocity, temperature and pressure. By knowing v_∞ and altitude, as function of time, together with an atmospheric model (U.S. Standard Atmosphere, 1976), it is possible to evaluate the free stream properties, such as p_∞ , T_∞ and c_∞ , which represent free stream pressure, temperature and speed of sound, respectively. For supersonic flow ($M_\infty > 1$), a detached shock wave appears ahead of the nose. By using the normal shock relationships, it is possible to calculate v_1 , T_1 and p_1 after the shock.

The heat flux over the external surface was calculated through the Zoby's method (Zoby et al, 1981; Miranda & Mayall, 2001), namely:

$$q = H (T_{aw} - T_w) \quad (1)$$

where q is heat flux, T_w is the wall temperature and T_{aw} is the adiabatic wall temperature, also called recovery temperature, T_r , given by:

$$T_{aw} = T_e + F_R \frac{v_e^2}{2c_p} \quad (2)$$

where c_p is the specific heat, T_e the temperature and v_e the velocity. The subscript e refers to conditions at the boundary layer edge. F_R is the recovery factor, equal to $\sqrt{Pr_w}$, for laminar flow and $\sqrt[3]{Pr_w}$ for turbulent flow. Pr_w is the Prandtl number evaluated at wall temperature, $Pr_w = 0.71$. The convective heat transfer coefficient comes from the Reynolds analogy, namely:

$$H = 0.5 \rho_e c_p v_e Pr_w^{-a} C_F \quad (3)$$

where a is equal to 0.6 for laminar flow and 0.4 for turbulent flow. To take into account compressibility effects, a modified friction factor is obtained (Anderson, 1989)

$$C_F = K_I (Re_\theta)^{K_2} \left(\frac{\rho_e^*}{\rho_e} \right) \left(\frac{\mu_e^*}{\mu_e} \right)^{K_3} \quad (4)$$

In the equation above, Re_θ is the Reynolds number, based on the boundary layer thickness, θ

$$Re_\theta = \frac{\rho_e V_e \theta}{\mu_e} \quad (5)$$

H. A. Machado, M. Pires, R. F. Miranda, G. B. Ameloti
Structurally Integrated Thermal Protection Applied in the SARA

The superscript “*” refers to properties evaluated at Eckert’s reference temperature (T_e^*). Viscosity, μ , is evaluated according to Sutherland’s equation, as function of temperature (Anderson, 1989) and ρ is the specific mass. In Eq.(4) $K_1 = 0.44$, $K_2 = -1$ and $K_3 = 1$, for laminar flow. For turbulent flow, $K_2 = K_3 = -m$, and

$$K_1 = 2 \left(\frac{I}{C_5} \right)^{\frac{2N}{N+1}} \left[\frac{N}{(N+1)(N+2)} \right]^m \quad (6.a)$$

$$m = \frac{2}{N+1} \quad (6.b)$$

$$C_5 = 2.2433 + 0.93N \quad (6.c)$$

$$N = 12.76 - 6.5 \log_{10}(Re_\theta) + 1.21 [\log_{10}(Re_\theta)]^2 \quad (6.a)$$

For laminar flow, the boundary layer thickness is given by (Anderson, 1989):

$$\theta_L = \frac{0.664 \left(\int_0^y \rho_e^* \mu_e^* v_e R^2 dy' \right)^{\frac{1}{2}}}{\rho_e v_e R} \quad (7)$$

where y is measured along the body’s surface and $y=0$ corresponds to the stagnation point, and R is a geometric parameter schematically shown in Fig. 5, where the curved red line represents the nose cap surface.

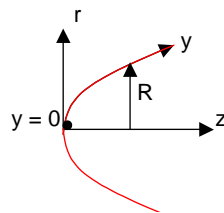


Figure 5. Coordinate system.

In this work the numerical integration of Eq. (7) was obtained according to the trapezoidal method. As $R \rightarrow 0$, Eq. (7) becomes undetermined. By taking the limit of Eq. (7) as $R \rightarrow 0$, the following expression is obtained (Miranda & Mayall, 2001):

$$\theta_L = \frac{0.332 (\rho_e^* \mu_e^*)^{\frac{1}{2}}}{\rho_e \sqrt{\frac{1}{R_N} \left[\frac{2(p_s - p_\infty)}{\rho_s} \right]^{\frac{1}{2}}}} \quad (8)$$

In this work Eq. (8) is applied for $y < 0.1 R_N$, where R_N is the radius of curvature at the stagnation point.

The boundary layer thickness for turbulent flow is obtained by solving the following first order differential equation:

$$\frac{D(\rho_e v_e R \theta_T)}{Dy} = 0.5 C_F \rho_e v_e R \quad (9)$$

After obtaining the boundary layer momentum thickness, θ , Re_θ , C_F and H can be evaluated by using Eqs. (5), (4) and (3), respectively. Along the transition region between laminar and turbulent flow, the following relationship is used¹¹:

$$q_{Tr} = q_L + F(y)(q_T - q_L) \quad (10)$$

where the subscripts Tr , L and T represent, respectively, transitional, laminar and turbulent flow. The transitional factor, $F(y)$, is given by (Dhavan & Narasinha, 1958):

$$F(y) = 1 - \exp\left\{-0.412\left[\frac{4.74(y - y_L)}{(y_T - y_L)}\right]\right\} \quad (11)$$

Transition is supposed to occur for $163 < Re_\theta < 275$.

Properties evaluation at the boundary layer edge is performed assuming isentropic flow between the stagnation region and the location “ t ” where properties are needed, namely

$$\rho_{e,i} = \rho_s \left(\frac{p_{e,i}}{p_s}\right)^{\frac{1}{\gamma}}; \quad h_{e,i} = h_s \left(\frac{p_{e,i}}{p_s}\right)^{\frac{\gamma-1}{\gamma}}; \quad v_{e,i} = \sqrt{2(h_s - h_{e,i})}; \quad T_{e,i} = \frac{h_{e,i}}{c_p} \quad (12)$$

The local pressure, $p_{e,i}$, is obtained from the modified Newton’s method (Anderson, 1989; Machado & Villas-Boas, 2006) and $\gamma=1.4$. The results of both methods are then compared. The subscript “ s ” appearing in Eqs. (12) refers to the stagnation condition. Eckert’s reference temperature is obtained from (Anderson, 1989):

$$\frac{T_{e,i}^*}{T_{e,i}} = 1 + 0.032M_{e,i}^2 + 0.58\left(\frac{T_w}{T_{e,i}} - 1\right) \quad (13)$$

The solution procedure can be summarized as follows:

1. From a given trajectory the US Standard Atmosphere (1976) is used to obtain the free stream properties, including the stagnation ones;
2. Normal shock relationships are used to obtain the fluid flow properties behind the shock;
3. By using the modified Newton method, pressure distribution is obtained along the payload;
4. Equations (12) provide the local properties at the boundary layer edge;
5. If $y < 0.1 R_N$, Eq. (8) provides the laminar boundary layer thickness, leading to the estimation of Re_θ , C_F and H , provided by Eqs. (5), (4) and (3), respectively;
6. If $y > 0.1 R_N$ and $Re_\theta < 163$, Eq. (7) is numerically integrated up to the location where the momentum thickness is to be estimated. Such an integration is performed by using the trapezoidal method;
7. If $y > 0.1 R_N$ and $Re_\theta > 275$, Eq. (9) is numerically integrated by the trapezoidal rule leading to the turbulent boundary layer thickness;
8. If $y > 0.1 R_N$ and $163 < Re_\theta < 275$, Eqs. (10) and (11) are used to estimate H ;

It should be pointed out that such a procedure is performed along the payload’s surface (following the y -coordinate), for different trajectory times. Therefore, $H=H(y,t)$.

2.2 Heat conduction in the porous media

Once the convection heat transfer coefficient and the adiabatic wall temperature are known, wall temperature distributions can be obtained. For the previous arrangement of thermal protection, is a simple heat conduction problem. Since the wall is made with Aluminium, which has a high thermal diffusivity, it can be treated as a one-dimensional problem along the wall thickness (Machado, 2006).

The Safil thermal conductivity was obtained from the model of Daryabeigi (2003) for heat conduction in porous media. The mathematical model used is detailed described in Daryabeigi’s work. The model considers the heat transfer between two parallel plates, combining the radiation and conduction modes. The fibrous insulation between the plates is considered a participating media. The main equation resulting from the assumptions is the one-dimensional energy conservation equation, with a source term for the radiation heat transfer.

$$\rho c \frac{\partial T}{\partial t} = \frac{\partial}{\partial y} \left(k_c \frac{\partial T}{\partial y} \right) - \frac{\partial q_r''}{\partial y} \quad (14)$$

For an optically thick medium, the diffusion approximation can be used resulting in the radiant heat flux of:

$$q_r'' = -k_r \frac{\partial T}{\partial y} \quad (15)$$

Using this approximation, the energy equation reduces to:

H. A. Machado, M. Pires, R. F. Miranda, G. B. Ameloti
Structurally Integrated Thermal Protection Applied in the SARA

$$\rho c \frac{\partial T}{\partial t} = \frac{\partial}{\partial y} \left(k_{eq} \frac{\partial T}{\partial y} \right) \quad (16)$$

where k (apparent or effective thermal conductivity) is obtained by superposition of the thermal conductivities due to solid conduction, gas conduction, and radiation:

$$k_{eq} = k_r + k_s + k_g \quad (17)$$

The radiant thermal conductivity for fibrous insulations, k_r , is provided by:

$$k_r = \frac{16 \sigma n^{*2} T^3}{3 \rho e} \quad (18)$$

where e is specific extinction coefficient; estimated from the experimental data using a genetic algorithm-based parameter estimation technique and n^* is the effective index of refraction. A curve fit of the effective index of refraction with fiber volume fraction was used. The optical thickness is given by $\tau = \rho.e.L$. The insulation can be considered optically thick only if $\tau \gg 1$, which is valid for insulation samples used in this study with optical thickness > 20 .

The solid conduction term, k_s , is extracted from an empirical model based on density and k of bulk material:

$$k_s(T) = F_s f_v^b k_s^*(T) \quad 1 \leq b \leq 3 \quad (19)$$

where F_s is a factor relating micro-scale geometric effects of fiber matrix and bulk dimensions. It is obtained from steady state measurements in vacuum and at cryogenic temperatures (test condition with negligible gas conduction and reduced radiation).

The heat conduction is considered to occur in the porous media, as a combination of the solid and gas conduction processes. The solid conduction occurs through the fibrous, and its thermal conductivity dependence with temperature is considered to be well known.

According to statistic thermodynamics, gas thermal conductivity is supposed to depend only on the temperature and to be independent on the pressure. However, in a porous media, it was verified that pressure plays an important role below a certain level.

The current model uses a classical approach to estimate the gas thermal conductivity inside the fibrous, based on the Knudsen hypothesis. The standard temperature function used to estimate the gas thermal conductivity, $k_{g0}(T)$, is corrected through the following equation¹:

$$k_g = \frac{k_{g0}(T)}{\Phi + 2\Psi \frac{\beta}{Pr} Kn} \quad (20.a)$$

Where:

$\Phi = 1, \Psi = 0$ for $Kn < 0.01$	(Continuum regime)
$\Phi = 1, \Psi = 1$ for $0.01 < Kn < 10$	(Transition regime)
$\Phi = 0, \Psi = 1$ for $Kn > 10$	(Free-molecular regime)

$$\beta = \left(\frac{2-\alpha}{\alpha} \right) \left(\frac{2\gamma}{\gamma+1} \right) \quad (20.b)$$

α is the thermal accommodation coefficient and γ is the gas specific heat ratio, Pr is the Prandtl number and Kn is the Knudsen number:

$$kn = \frac{\lambda}{L_c} \quad (21)$$

λ is the molecular mean free path of the gas, and L_c is the characteristic length of the fibrous insulation.

According to this model, the variation of K_{eq} as function of pressure and temperature difference between the plates (with a lower temperature of 60° C, which is the limit for the internal surface) is showed in Fig. 6. Both variations can be fitted by following function:

$$K_{eq}(\Delta T, P) = F(P) \cdot G(\Delta T) \quad (22.a)$$

$$G(\Delta T) = b \cdot e^{a\Delta T} \quad (22.b)$$

where $a = 0.001884858198$ and $b = 0.03446775065$.

$$F(P) = b \cdot P^a \quad (22.c)$$

where $a = 0.005102720025$ and $b = 0.03910708429$. This function allows obtaining an overall *rms* error of 1.33 %.

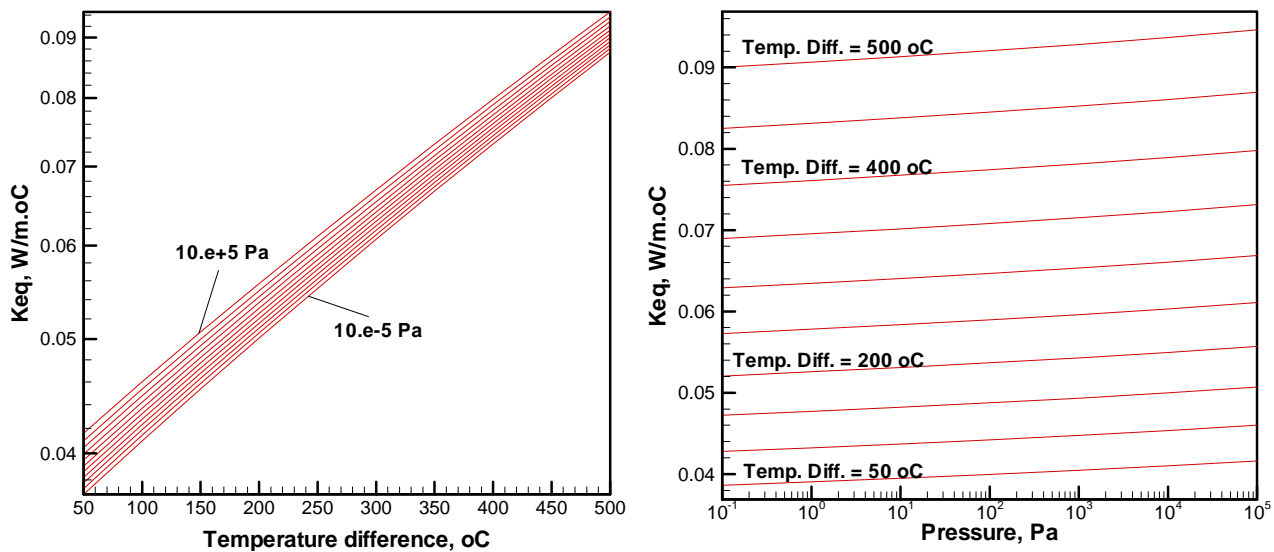


Figure 6. Results for K_{eq} as function of pressure and temperature difference.

In order to extract the other physical properties of the porous media, the following equations were employed:

$$C_{p_{air}} = 1027.582 - 0.2216 T + 4.561 \times 10^{-4} T^2 + 2.455 \times 10^{-7} T^3 - 16.643 \times 10^{-10} T^4 + 3.616 \times 10^{-13} T^5 - 6.349 \times 10^{-17} T^6 \quad (23)$$

$$K_{air} = -1.8763 \times 10^{-3} + 1.218 \times 10^{-4} T - 1.328 \times 10^{-2} T^2 + 1.479 \times 10^{-10} T^3 - 18.58 \times 10^{-14} T^4 + 1.705 \times 10^{-17} T^5 + 9.527 \times 10^{-22} T^6 \quad (24)$$

$$K_s = (1.63 \times 10^{-5} - 2.114 \times 10^{-8} T + 1.131 \times 10^{-11} T^2 - 2.094 \times 10^{-15} T^3) \times \rho \quad (25)$$

where ρ is the density of the porous material. In this work, ρ was considered to be 24.2 kg/m³. The physical properties for the other materials are showed in Tab. 1.

Table 1. Physical properties of structural and TPS materials.

Property	Material	
	Aluminium	cork
ϵ - Emissivity	0.06	0.78
C_p - Specific heat (J/kg K)	960	1971.8
K - Thermal conductivity (W/m K)	177	0.084
ρ - Density (kg/m ³)	2710	480

3. RESULTS

The variations of the convective heat transfer coefficient (H) and the recovery temperature (T_r) with the y -coordinate for several times are showed in Fig.7. The variation of the convective coefficient becomes smooth after the semi-spherical section (about $y = 0.4$ m), and the recovery temperature behaves as a function of time, being independent of position what allows to interpolate average values for both parameters in the conic section. The variation of these averages and the fitting curves are showed in Fig. 8.

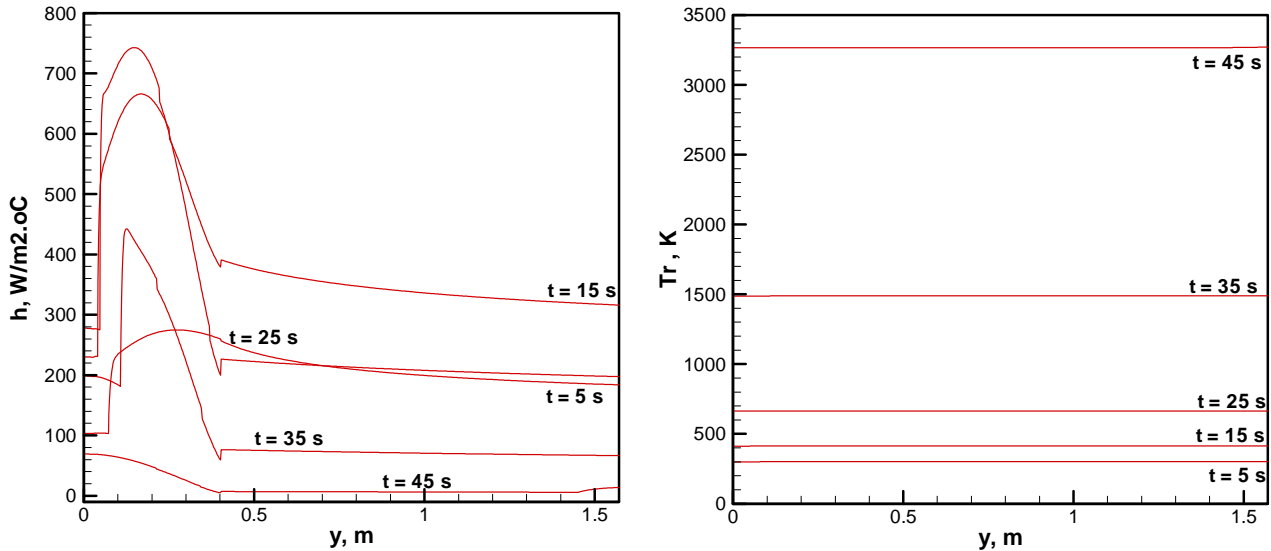


Figure 7. Convective heat transfer coefficient and recovery temperature during SARA trajectory.

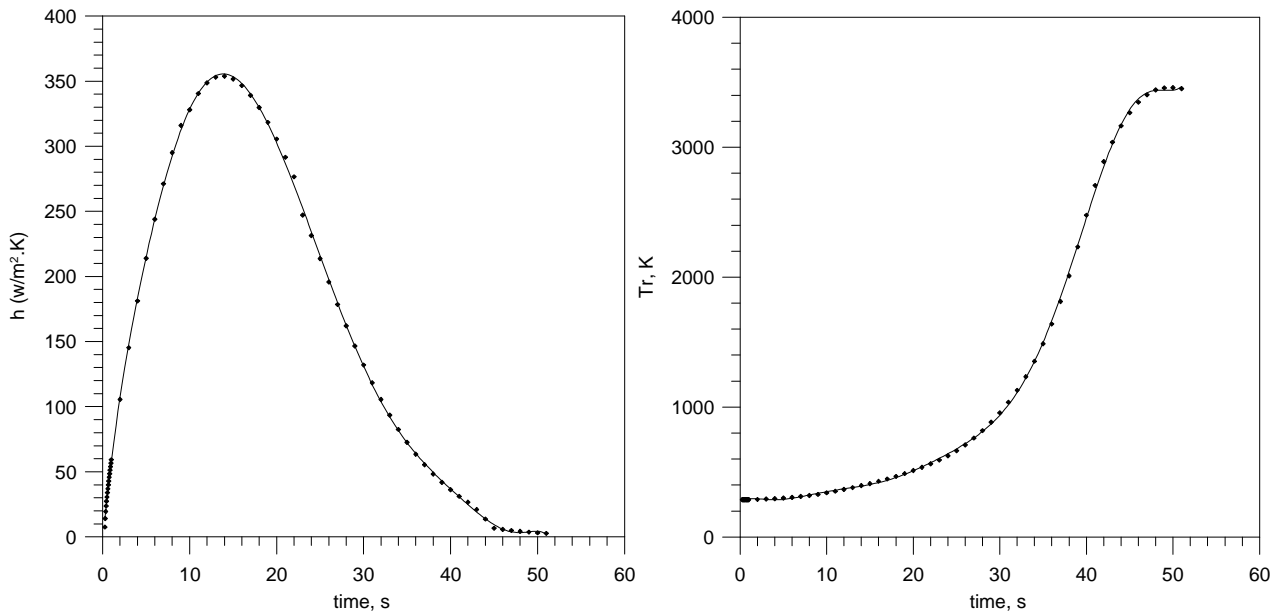


Figure 8. Average convective heat transfer coefficient and recovery temperature in the conic section during SARA trajectory.

The Finite Volume Method is employed to solve the one-dimensional energy conservation equation (Eq. 14), in order to obtain the temperature profiles within the wall thickness. The boundary conditions for the internal and external surfaces, $x = 0$ and $x = L$, respectively, are adiabatic wall and convective heat exchange.

Figure 9 shows the temperature variation with the time in internal and external surfaces of the conic section, for both types of TPF. Although the maximum internal temperature rises slightly, from $27.53^\circ C$ in the conventional TPS to $29.20^\circ C$ in TISSC configuration, the last one presented a better thermal insulation, with a maximum temperature of $593.82^\circ C$, against $621.56^\circ C$ in the conventional TPS (with a peak of $823.52^\circ C$). In spite of the effect of ablation in cork has been neglected (since this is designed as a recoverable vehicle), these results indicates that TISSC is able to

assure the same insulation capacity of the conventional TPS, since in both cases the internal temperature was kept well below the limit of 60° C.

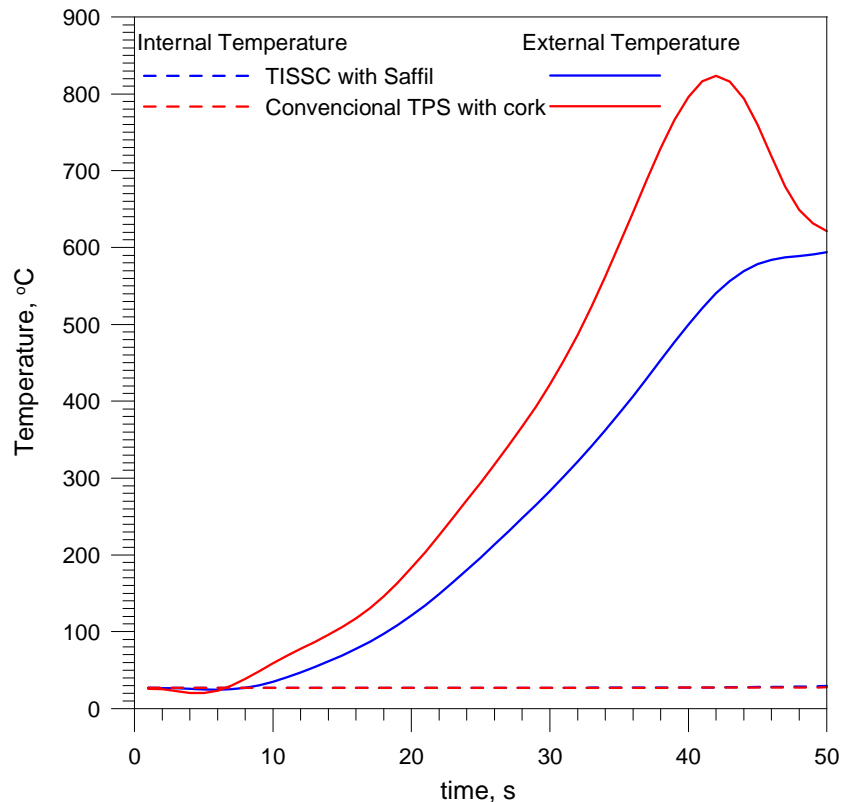


Figure 9. Temperature variation with the time in internal and external surfaces for both TPS configurations.

The weight per surface unit in every type of TPS can be estimated with the values of each material density and layer thickness, already presented. A quick estimation gives 134,6 N/m² for the conventional cork TPS and 84,0 N/m² for the TISSC with Saffil, which means a reduction of 37.6 % in the total weight of the conic section wall. Besides the weight reduction, it should be noted that the TISSC structure is considerable more rigid than the conventional arrangement for the vehicle wall.

Even considering that the maximum TISSC temperature surpasses the temperature limit for safe use of the Aluminium, the use of TISSC is feasible through other materials, like composites, ceramics or metals (steel, titanium or special alloys).

4. CONCLUSION

In this work, the thermal performance of Thermally Integrated Structural Sandwich Core (TISSC) was compared with the conventional TPS when applied in the conic section of the SARA Suborbital platform. The Zoby's Method was employed to estimate the convection heat transfer over the external wall during the trajectory. The temperature dependence of the apparent thermal conductivity for the porous fulfillment in the TISSC (Saffil) was constructed using the results provided through the model proposed by Daryabeigi. The results for the external and internal surface temperatures showed the TISSC viability as a TPS for the SARA recoverable vehicle, with advantages in weight reduction and strength improvement, since the convenient material is chosen. An economic analysis is strongly recommended for future works.

5. ACKNOWLEDGEMENTS

Authors would like to thank CNPq and AEB (Brazilian Space Agency) for the financial support during this work.

H. A. Machado, M. Pires, R. F. Miranda, G. B. Ameloti
Structurally Integrated Thermal Protection Applied in the SARA

6. REFERENCES

- Anderson Jr., J.D., *Fundamentals of Aerodynamics*, McGraw-Hill, New York, 1990.
- Anderson Jr., J.D., *Hypersonic and High Temperature Gas Dynamics*, AIAA Education Series, AIAA, New York, 1989.
- Daryabeigi, K., "Heat Transfer in High Temperature Fibrous Insulation", *Journal of Thermophysics and Heat Transfer*, Vol. 17, No. 1, January-March, 2003.
- Machado, H. A., 2006, "Thermal Protection for Aerodynamic Heating in the SARA Sub-orbital Platform", *Proceedings of the IV National Congress of Mechanical Engineering – CONEM*, Recife, Brazil (in Portuguese).
- Machado, H.A. and Villas-Boas, D.J.F., "Comparative Study of Models for Aerodynamic Heating of Space Vehicles," *Proceedings of Brazilian Thermal Sciences Meeting [CD-ROM]*, Curitiba, Brazil, 2006 (in Portuguese).
- Martinez, O. A.; Bapanapalli, S.; Sankar, B., Haftka, R. and Blosser, M., Micromechanical Analysis of Composite Truss-Core Sandwich Panels for Integral Thermal Protection Systems, *47th AIAA/ASME/ASCE/AHS Structures, Structural Dynamics and Materials Conference*, Newport, RI, 2006.
- Miranda, I.F. and Mayall, M.C de M., 2001, *Convective Heat Flux in Micro-Satellites during the Atmospheric Reentry*, Graduate Dissertation, Air Force Technical Institute - ITA, São José dos Campos, Brazil (in Portuguese).
- Moraes Jr., P., 1998, "Design Aspects of the Recoverable Orbital Platform SARA", *Proceedings of 8th Chilean Congress of Mechanical Engineering*, Concepción, Chile.
- U.S. Standard Atmosphere, 1976.
- Zoby, E.V., Moss, J.N. and Sutton, K., 1981, "Approximate Convective Heat Equations Hypersonic Flows", *Journal of Spacecraft and Rockets*, Vol. 18, No. 1, pp. 64-70.

7. RESPONSIBILITY NOTICE

The authors are the only responsible for the printed material included in this paper.